ISSN 2075-1133, Inorganic Materials: Applied Research, 2020, Vol. 11, No. 4, pp. 801–808. © Pleiades Publishing, Ltd., 2020.
Russian Text © The Author(s), 2019, published in Materialovedenie, 2019, No. 10, pp. 10–18.

High-Sensitivity Measurements of the Magnetic Properties of Materials at Cryogenic Temperatures

D. A. Velikanov*

Kirensky Institute of Physics, Krasnoyarsk Scientific Center, Siberian Branch, Russian Academy of Sciences, Krasnoyarsk, 660036 Russia

**e-mail: dpona1@gmail.com*

Received December 24, 2018; revised March 29, 2019; accepted June 6, 2019

Abstract—An original magnetometer based on a dc superconducting quantum interferometer is described. The design features of the device are discussed and functional diagrams of its new units are presented. The magnetic moment measurement methods that optimize the measurement process are proposed. Examples of the investigations carried out on the samples of different materials are given. The factors affecting the reliability of the magnetic measurements are considered.

Keywords: quantum interferometer, magnetometer, dynamic range, magnetic moment, magnetization

DOI: 10.1134/S2075113320040413

INTRODUCTION

The advances in physics of magnetic phenomena are related, to a great extent, to the instrumentation available to researchers. In the magnetic measurements of small samples, of great importance is the effective transmission of the magnetic flux induced by the magnetic moment of a sample to a magnetically sensitive element of a device. The best methods for this purpose are based on using vibrating sample and SQUID (superconducting quantum interference device) magnetometers [1]. The latter, unsurpassed in sensitivity, are widely used in the magnetic susceptibility measurements in the temperature range from helium to room temperature. At present, commercial magnetometers are available to experimentalists; however, original designs make it possible to introduce engineering solutions that would allow one to avoid the drawbacks of commercial devices. In addition, it becomes possible to carry out original investigations.

SQUID Magnetometer

The device developed at the Kirensky Institute of Physics, Siberian Branch, Russian Academy of Sciences (Fig. 1), is designed to study the magnetic properties of a wide range of materials, from strongly magnetic ferro- and ferrimagnets to spin glasses, multilayer films, and nanostructures. As a magnetic flux detector, it uses SQUID *1*. A useful signal is transmitted from sample *2* to the SQUID by a short-circuited superconducting magnetic flux transformer containing two opposite receiving coils *3* and *4* and SQUID input coil *5*. The gradiometric connection of coils *3* and *4* facilitates the effective suppression of magnetic interference. The SQUID (through the matching *LC* circuit) and modulation and feedback coil *6* are connected to electronics module *7*, in which the useful signal is amplified and processed and signals supplied to coil *6* are formed.

The cryogenic part of the magnetometer consists of a cryostat based on glass Dewar flasks for cryogenic agents connected to pumping and gas communications and a cryogenic insert. Superconducting solenoid *8* inducing a magnetizing field operates in a short-circuited mode. The solenoid and the flux transformer are equipped with heaters *9* and *10*, which convert sections of the superconducting circuits to the normal state for the time of variation in the magnetizing field. The solenoid is fed by bipolar current source *11* with three field subranges of 0.000...±0.004 T, 0.00...±0.04 T, and 0.0...±0.15 T.

The helium bath volume is 0.0012 m^3. Owing to some design features of the cryostat, its heat-insulating properties remain invariably high; moreover, there is no need for periodic maintenance work with the Dewar flask for liquid helium. In addition, the design of the cryogenic part excludes the occurrence of destructive stresses in the walls of the Dewar flask upon cooling and reduces the loss of the expensive cryogenic agent.

Sample *2* is placed in an anti-Dewar and heat-insulated from a helium bath with a vacuum jacket. The sample temperature can be controlled within 2–370 K using a differential Au/0.07% Fe–Cu thermocouple. Working junction *12* of the thermocouple is located near the sample and control junction *13* is located in

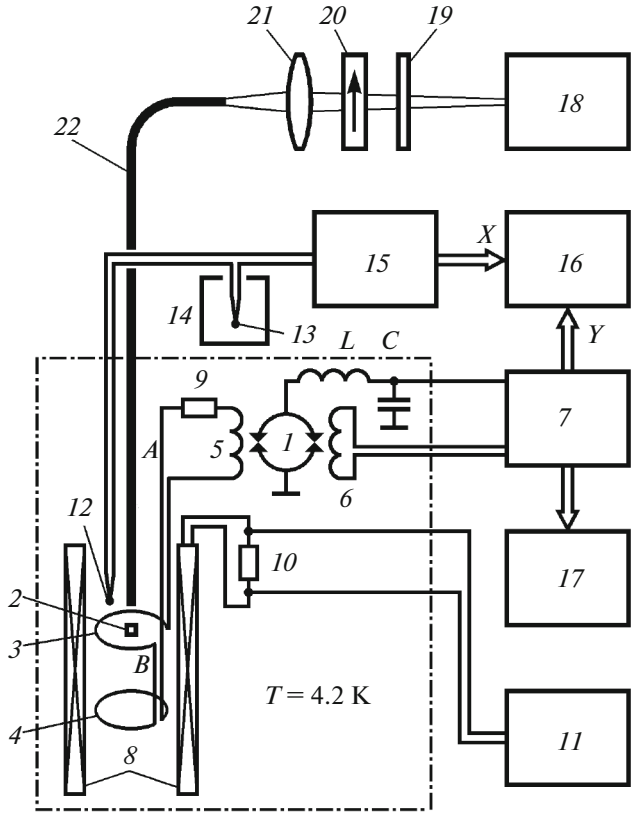

Fig. 1. General experimental configuration of a SQUID magnetometer: (*1*) SQUID, (*2*) sample, (*3*, *4*) receiving coils, (*5*) SQUID input coil, (*6*) modulation and feedback coil, (*7*) SQUID electronics module, (*8*) superconducting solenoid, (*9*, *10*) heaters, (*11*) current source, (*12*, *13*) thermocouple junctions, (*14*) thermostat, (*15*) electronics module, (*16*) recording device, (*17*) oscilloscope, (*18*) radiation source, (*19*) modulator, (*20*) attenuator, (*21*) condenser, (*22*) light guide.

thermostat *14*, in which the temperature is stabilized at 323 K. In electronics module *15*, the nonlinear thermo emf of the thermocouple is first amplified and then processed by the ADC–ROM–DAC (analog-to-digital converter–read-only memory–digital-to-analog converter) circuit. A 12-bit ROM is programmed for the thermocouple type used. The dc voltage formed at the output of module *15* is directly proportional to the absolute temperature of the sample.

Electronics modules *7* and *15* are connected to recording device *16*. Oscilloscope *17* is used to tune the magnetometer and visually control its operation. The dynamic range of the SQUID magnetometer is 2×10^{-11}–5×10^{-5} A m^2.

In addition, the magnetometer is equipped with an optical path containing optical radiation source *18*, electromechanical light flux modulator *19*, attenuator *20*, condenser *21*, and fiber-optic light guide *22*. This makes it possible to perform high-sensitivity measurements of the photoinduced changes in the magnetic moment of photosensitive crystals. In studying the time behavior of photoinduced signals, the input *X* of recording device *16* is connected to a time base unit.

SQUID Electronics

The maximum sensitivity of the magnetometer is obtained using SQUIDs in the null-detection mode (the flux-locking system). The operation of a SQUID in this mode is based on the periodic dependence of the SQUID voltage on the magnetic flux applied to its contour [1]. For servicing a dc SQUID, an electric circuit was developed and fabricated; its main components are presented in Fig. 2. A prototype for this circuit was the circuit described in [2], but significantly renewed. In the flux-locking system, the feedback current is supplied through resistor R_{OC} to modulation coil L_M, maintaining a constant quasistatic magnetic flux through the interferometer circuit. In this case, the change in the input flux corresponds to the voltage increment at the integrator output.

In the prototype proposed in [2], the measurement process stops as soon as the integrator saturates. This limitation can be overcome by equipping the electric circuit with a magnetometer volume range expander (Fig. 3a), which monitors the voltage at the integrator output. When this voltage exceeds the limits set by reference voltage source *1*, dual-limit regenerative comparator *2* switches and triggers univibrator *3* on a D trigger, which controls electronic switch *4*. Closing the switch causes the integrator to reset to zero. In this case, the comparator switches to the initial state and

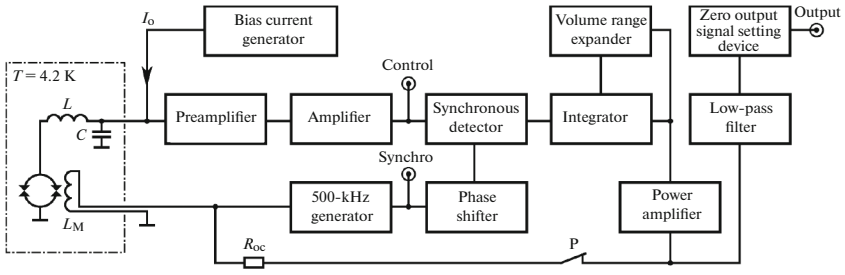

Fig. 2. Electronics of dc SQUID.

the flux induced by the current in the feedback circuit and applied to the SQUID changes stepwise by an integer number of magnetic flux quanta. Thus, the expander makes it possible (i) to increase the dynamic range of the SQUID magnetometer toward the upper limit without changing the absolute sensitivity of the device, (ii) automatize the integrator reset operation, and (iii) exclude manual actions by an operator.

Another functional device is designed to minimize the effect of the variation in the magnetic moments of components of the cryogenic insert. Using a zero output signal setting device (Fig. 3b), the zero voltage is set at the magnetometer output before recording each experimental point. This device contains a voltage repeater, a sample-and-hold circuit, and a differential amplifier. It has two modes of operation: zero setting and measurement. The modes are switched with electronic switch K1, which is controlled by an operator using toggle P1. The zero output signal setting device ensures the short time (~10^{-3} s) and high zero output signal setting accuracy (~0.02% of the top limit of the dynamic range on each of the three available measurement limits). The zero output signal setting device makes it possible to exclude the zero setting unambiguity of manual operations, which reduces the measurement error.

The SQUID electronics consists of two design modules. All the functional units, except for a preamplifier, are mounted inside the instrument mainframe 0.48 × 0.36 × 0.1 m^3 in size. The preamplifier is located in a cylindrical titanium housing with a diameter of 0.032 m and a height of 0.08 m fixed on a cryostat cup and connected to the main unit with a cable.

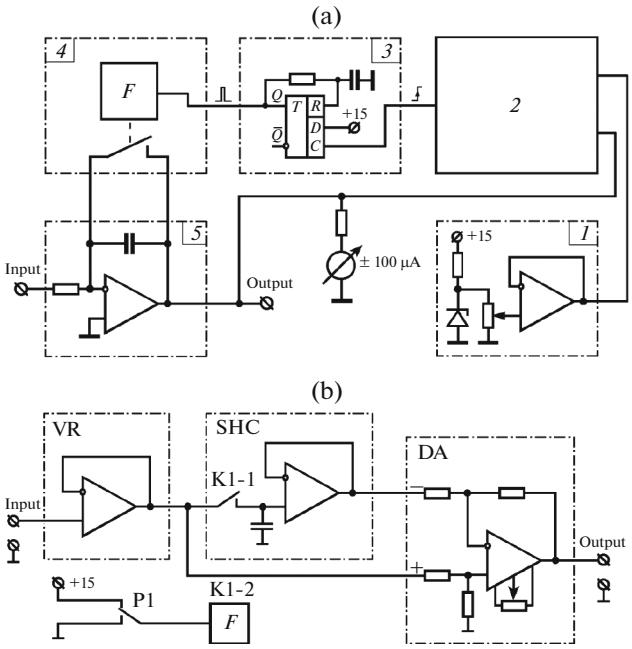

Fig. 3. (a) Volume range expander: (*1*) reference supply source, (*2*) two-threshold regenerative comparator, (*3*) univibrator, (*4*) electronic switch, (*5*) connection of the electronic switch to the integrator. (b) Zero output signal setting device: voltage repeater (VR), sample-and-hold circuit (SHC), and differential amplifier (DA).

Methods for Measuring the Magnetic Moments

The following methods have been developed to optimize the magnetic measurements on the SQUID magnetometer.

1. Measurements of the static magnetic properties of the samples the magnetic moment of which is below the upper limit of the magnetometer measurements. Sample *2* (Fig. 1) fixed in a holder at the rod end is placed at a distance from receiving coils *3* and *4* on the top (position *A*). Using the zero output signal setting device, the voltage at the output of the SQUID magnetometer is set to zero. Then, the sample is smoothly moved down to a position somewhat lower than upper receiving coil *3* (position *B*). When the sample is moved, the magnetic flux through the receiving coils and, consequently, through SQUID input coil *5* changes. The magnetometer output voltage U proportional to the magnetic flux variation and depending on the sample position (Fig. 4a) attains its maximum U_{max} when the sample passes near the center of coil *3*. The magnetic moment m of the sample is determined as

$$m = kU_{max} - m_h,$$

where k is the magnetometer constant measured at the calibration of the device and m_h is the contribution of the empty sample holder.

2. Measurements of the static magnetic properties of the samples the magnetic moment of which is higher than the upper limit of the SQUID magnetometer measurements. These measurements are performed mainly when recording the temperature dependences of the magnetic moment $m(T)$. The sample under investigation is cooled down to the helium temperature, its position is adjusted to the maximum output signal of the magnetometer, and then the sample is fixed. Next, the sample is heated and, simultaneously, the continuous recording of the output signal of the device is switched on. When the voltage goes beyond the set limits, the voltage range expander zeroes the integrator and the experimental curve continues to be recorded. Note that the recorded $m(T)$ dependence consists of several portions, which must be joined together to obtain a desired experimental curve.

3. Measurements of the photoinduced changes in the magnetic moment, which is necessary for photomagnetic crystals. In this case, the time dependences of the magnetic moment ($m(t)$) are recorded. Before the measurements, the sample is set to the maximum output signal of the magnetometer and fixed. Using modulator *19* (Fig. 1), light pulses are generated (curve *1* in Fig. 4b), which pass through optical fiber

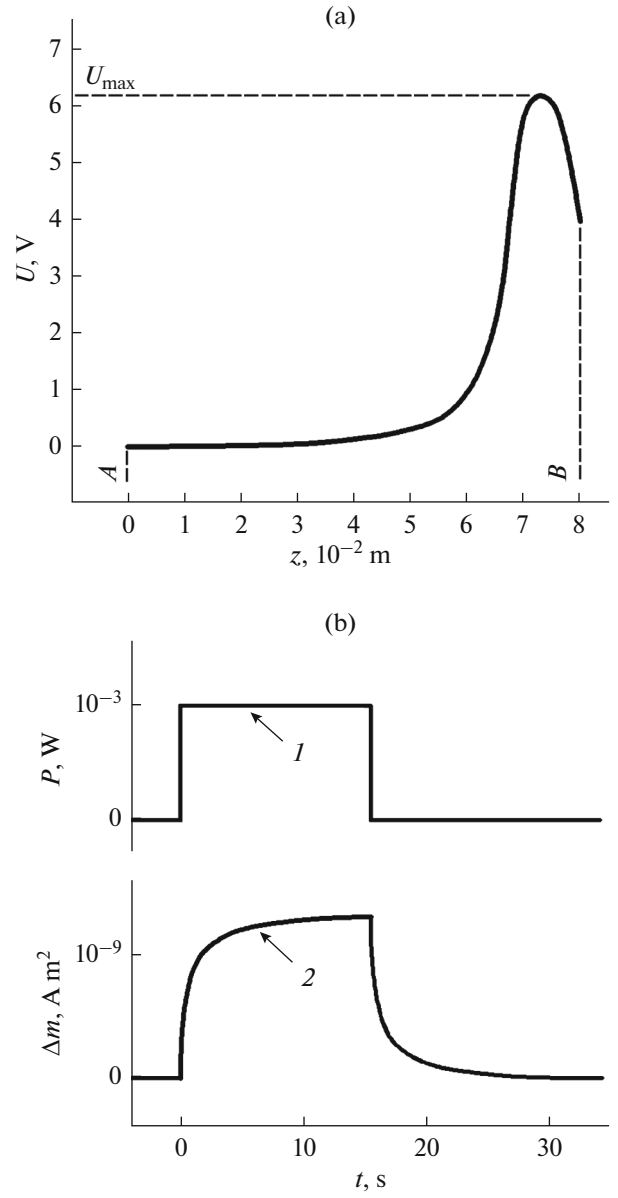

Fig. 4. (a) Dependence of the output voltage of the SQUID magnetometer on the sample position. (b) Photomagnetic measurements. (*1*) Optical radiation pulse and (*2*) photoinduced change in the magnetic moment.

22 and irradiate the sample. In this case, a signal proportional to the change Δm in the magnetic moment of the sample is induced in the receiving coils (curve *2* in Fig. 4b). The supplied radiation power P is tuned by attenuator *20*.

Fundamental Study of the Magnetic Properties

Below, we give some examples of the fundamental investigations carried out on the above-described physical instrument. It is worth noting that the objective study of the properties of natural minerals is complicated by the presence of various impurities. Therefore, artificially grown single-crystal analogs are preferred, since, in this case, the substances are more likely pure. Below, we present the data of the magnetic measurements of several magnetically interesting weak-magnetic materials; some of them were first synthesized at the Kirensky Institute of Physics, Siberian Branch, Russian Academy of Sciences.

Noncollinear Antiferromagnet

The magnetic susceptibility χ of the CuB_2O_4 copper metaborate tetragonal single crystals at temperatures of $T > 21$ K obeys the Curie–Weiss law, while at $T < 21$ K, the susceptibility is strongly anisotropic (Fig. 5a) [3]. When the magnetic field is perpendicular to the crystallographic c axis, the $\chi(T)$ dependence at temperatures of $T = 21$ and 10 K exhibits pronounced anomalies. At the same orientation, in the range of $10\ \text{K} < T < 21$ K, there is a sharp kink in the magnetic field dependences of the magnetization $\sigma(B)$, the position of which depends on temperature (Fig. 5b). This indicates that, in the temperature range of $10\ \text{K} < T < 21$ K, the CuB_2O_4 crystal passes to the weak-ferromagnetic state induced by an external magnetic field and the magnetic moments of the sublattices lie in the basal crystal plane.

Anisotropic Spin Glass

The spin glass state is most frequently observed in polycrystalline materials, which are known to have isotropic properties. Therefore, of great interest is the anisotropic behavior of the spin glass state, which can take place in single crystals. Figure 6 shows the temperature dependences of the magnetization $\sigma(T)$ of the single-crystal β-$Cu_3Fe_4(VO_4)_6$ compound [4]. The magnetic measurements were performed in the two cooling modes: zero field cooling (ZFC) and cooling in a magnetic field (field cooling, FC). A sharp magnetization peak characteristic of spin glasses is related to the freezing temperature. It can be seen that the location of the peak essentially depends on the orientation of the single crystal relative to the magnetic field B and shifts from 10 to 2.5 K, depending on the measurement direction. Below the freezing temperature, there is a clear difference between the ZFC and FC dependences.

In addition, at $T = 4.2$ K, the relaxation of the thermoremanent magnetization is observed, the rate of which depends on the sample orientation. This is additional evidence for the fact that the β-$Cu_3Fe_4(VO_4)_6$ crystal is an anisotropic spin glass.

Kondo Compound

Let us consider the magnetic properties of the samples with the extremely low magnetic susceptibility

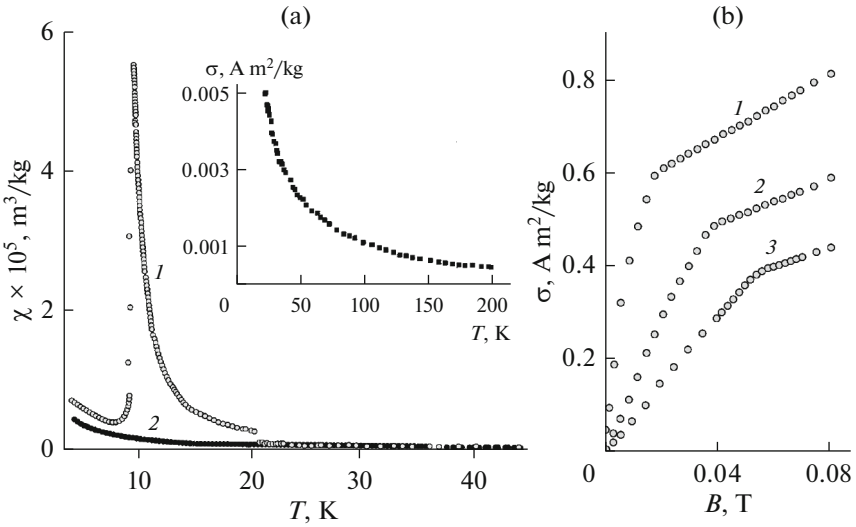

Fig. 5. Temperature dependence of the magnetic susceptibility of the CuB_2O_4 single crystal. (a) Magnetic field $B = 5 \times 10^{-3}$ T (*1*) perpendicular and (*2*) parallel to the crystal *c* axis. Inset: high-temperature portion of the temperature dependence of the magnetization. (b) Magnetic field dependences of the magnetization of the CuB_2O_4 single crystal at $T =$ (*1*) 10, (*2*) 13, and (*3*) 17 K at the orientation $B \perp c$.

($\chi \sim 10^{-8}$ m^3/kg), i.e., the ε-FeSi crystals. Both poly- and single crystals of the nonmagnetic ε-phase ferrosilicides were studied [5].

In studying the weak-magnetic materials, the quality of the results directly depends on the mass of the samples under investigation: the larger the mass, the higher the signal-to-noise ratio. For the magnetic measurements, it is desirable to prepare ε-FeSi samples with a mass of several hundred milligrams. However, with an increase in the polycrystal volume, the samples will probably contain magnetic inclusions, which are formed during the synthesis of materials as a result of imperfection of the technology. To improve the homogeneity of the composition of polycrystalline samples, it is necessary to perform magnetic rejection or multiply repeat the technological cycle. Single-crystal samples were small (~10^{-3} m) and therefore had a mass of several milligrams. The magnetic moment of the samples corresponds to their mass and size parameters and amounts to ε-FeSi ~ 10^{-10}–10^{-8} A m^2 in a field of $B = 0.01$ T, which approaches the magnetometer sensitivity limit. Therefore, these and other similar magnetic measurements require special accuracy and accounting for the signal from the empty holder.

In the FeSi crystals, iron ions are in the tetravalent state (Fe^{4+}) and have the ground low-spin state e_{2g}^4 ($S = 0$) in the d^4 configuration. The energy gap between the ground and first excited states is about ~600 K. Therefore, at low temperatures, the magnetic moment should be completely absent and only arise with increasing temperature as the high-spin state $e_{2g}^3 t_{2g}^1$ ($S = 1$) is populated. The maximum susceptibility $\chi(T)$ at $T = 500$ K is related just to the population of this level. The low-temperature features observed in the experiments (Fig. 7) were interpreted within the model of impurity centers. Fitting the experimental curves by the Langevin functions, the parameters of iron clusters occurring owing to the crystal nonstoichiometry were determined.

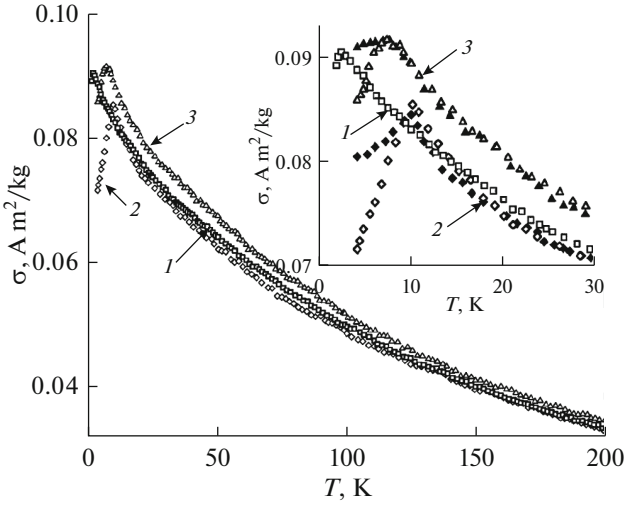

Fig. 6. Temperature dependence of the magnetization of the single-crystal β-$Cu_2Fe_4(VO_4)_6$ samples measured in a field of $B = 0.05$ T in three mutually perpendicular directions (*1*–*3*). Open symbols correspond to the ZFC mode and closed symbols correspond to the FC mode.

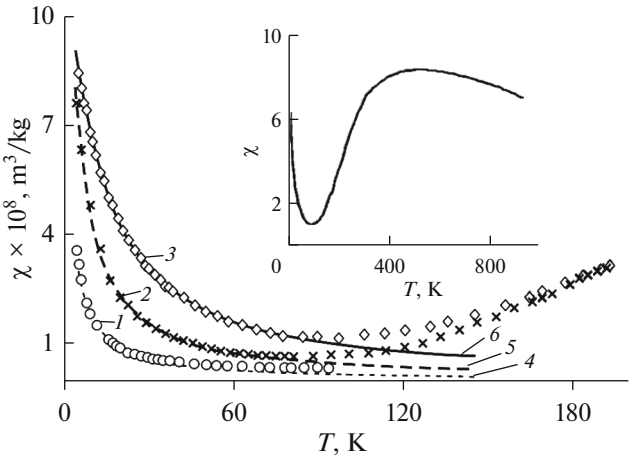

Fig. 7. Temperature dependence of the magnetic susceptibility $\chi(T)$ of the ε-FeSi crystals: polycrystals with different degrees of nonstoichiometry (*1*, *2*) and single crystal (*3*). Points *1*–*3* correspond to the experiment and lines *4*–*6* correspond to the theoretical fitting using the Langevin functions. The measuring field is $B = 0.06$ T. Inset: $\chi(T)$ dependence in the temperature range of 4.2–950 K.

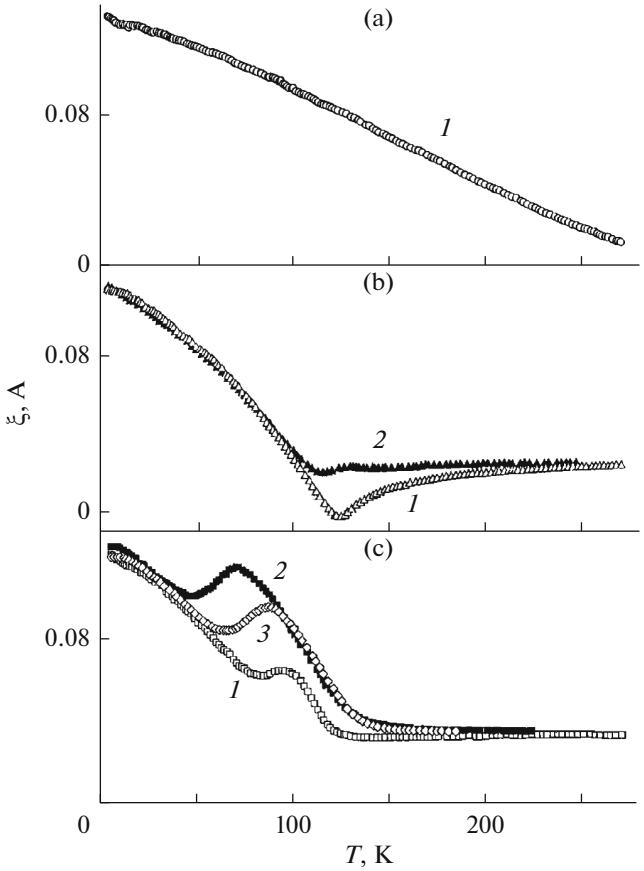

Fig. 8. Temperature dependences of the magnetization of the $(Gd/Si/Co/Si)_{20}$ multilayer nanostructures. (a) $t_{Si} = 0$, (b) 5×10^{-10} m, and (c) 10^{-9} m. $B = (1)$ 0.02, (*2*) 0.1, (*3*) 0.05 T. $t_{Co} = 3.5 \times 10^{-9}$ m and $t_{Gd} = 7 \times 10^{-9}$ m for all the nanostructures.

Multilayer Nanostructures

Study of the film systems containing ferromagnetic layers separated by semiconductor layers is interesting for controlling their magnetic characteristics by varying the parameters of the layers. In particular, the temperature dependence of the magnetization $\zeta(T)$ of the $(Gd/Si/Co/Si)_{20}$ multilayer nanostructures significantly depends on the silicon layer thickness t_{Si} [6]. (Here, the magnetization ζ is the magnetic moment of a unit film surface.) The formation of silicon spacers with a thickness of $t_{Si} = 5 \times 10^{-10}$ m leads to the occurrence of a compensation point on the $\zeta(T)$ dependence (curve *1* in Fig. 8b) and the appearance of a small maximum with an increase in the magnetic field B (curve *2* in Fig. 8b). At a silicon layer thickness of $t_{Si} = 10^{-9}$ m, the minimum magnetization, which can be attributed to the compensation point, is observed in fields of up to $B \sim 0.01$ T; in addition, with increasing field B, the maximum in the $\zeta(T)$ dependence grows and shifts to the low-temperature region (Fig. 8c). Such an unusual behavior of the magnetization is explained by the fact that the interaction of gadolinium layers with neighboring cobalt layers through a silicon spacer leads to the formation of a noncollinear magnetic structure in the form of a flat cone of the magnetic moments of the gadolinium layers. The total moment of the conical structure is antiparallel to the total magnetic moment of the cobalt layers. As the temperature increases, the cone of moments of the rare-earth subsystem collapses against the background of the decreasing total magnetic moment.

Reliability of the Results

The reliability of the experimental data obtained in the course of magnetic measurements determines the correctness of establishing the type of magnetic ordering in a material under study. It should be noted that, sometimes, especially at the initial stage of operation, users of commercial magnetometers, including, for example, the most widely used MPMS (Magnetic Property Measurement System) [7] and PPMS (Physical Property Measurement System) facilities, have an insufficiently clear idea of the processes that occur in these complex instruments during measurements. In particular, in the magnetometers with a superconducting solenoid, the magnetizing field sweep to several tesla is accompanied by the occurrence of magnetic flux pinning on inhomogeneities of a superconductor in the winding wire. As a result, magnetic vortices arise, which create internal magnetic fields; this ultimately leads to the occurrence of a residual field of 10^{-3}–10^{-2} T in the sample region [8]. This residual field is in no way taken into account, since the devices do not include a magnetic field sensor, and the field value is calculated on the basis of the measured current in the solenoid. Unfortunately, such nuances are not properly reflected in maintenance manuals. This

results in the occurrence of an uncontrolled instrumental error, which, during operation in weak fields, leads to errors in the measurements of the field and to the subsequent incorrect interpretation of experimental results.

Most frequently, researchers detect superconductivity where it does not exist [9–11]. In particular, a weak ferromagnetic moment in a negative field is mistaken for a manifestation of diamagnetism [9, 11]. For instance, when studying the temperature dependences of the magnetic moment of the weak-ferromagnetic $Ba_2Cu_3O_4Cl_2$ and $Sr_2Cu_3O_4Cl_2$ samples, the authors of [11] came to the conclusion about the occurrence of superconductivity in them at high (337 and 386 K, respectively) temperatures and even explained this "phenomenon." Meanwhile, they even did not take into account that the magnetic field dependences of the magnetization of high-temperature superconductors have a special characteristic form [12, 13].

Certainly, these and similar results seem extremely doubtful from their inception and require thorough reexamination. The magnetic measurements performed by the author at the insistent request of the "discoverers" have unequivocally proved that, in the above-mentioned materials, no transitions to the superconducting state with anomalously high critical temperature occurred [14]. Moreover, superconductivity in them is fully absent at low temperatures. In order to exclude the residual field in a superconducting solenoid, the measurements in weak fields were performed right after cooling the cryogenic part of the magnetometer to the liquid helium temperature.

In addition, it is erroneous to conclude that the temperature of the magnetic phase transition shifts depending on the rate of change in the temperature of the sample [11]. In reality, this "shift" is caused by the hardware error resulting from the temperature gradient in the magnetometer insert. The higher the sample heating rate, the greater the difference between the sample and sensor temperatures.

Photomagnetism

The MPMS-type magnetometers [7] are optionally equipped with an optical fiber for photomagnetic studies. It should be noted, however, that, since the MPMS measurement procedure is complex, the time required for obtaining one experimental point is 20 s or more. The sample is mechanically moved between the receiving coils and its total magnetic moment is measured. For this reason, the MPMS facility is suitable for studying only slow and fairly high-intensity photoinduced magnetization changes [15, 16].

The author's SQUID magnetometer has an operating speed higher by a factor of 1000 and can work in a continuous mode; therefore, it can detect much finer photomagnetic effects in dynamics (curve *2* in Fig. 4b). Thus, reversible photoinduced magnetization changes

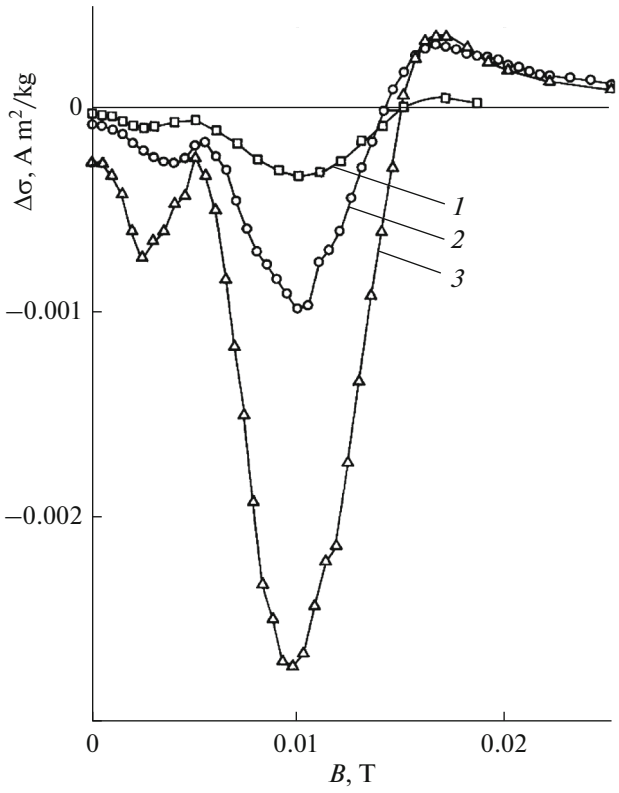

Fig. 9. Magnetic field dependences of the photoinduced change in the magnetization of the $FeBO_3$ crystal at optical pump power levels of (*1*) 2×10^{-6}, (*2*) 4×10^{-6}, and (*3*) 10^{-5} W/m^2. $T = 4.2$ K.

$\Delta\sigma$ were detected in the $FeBO_3$ iron borate crystals irradiated with laser light with a wavelength of $\lambda = 6.3 \times 10^{-7}$ m (Fig. 9) [17]. Note that the $\Delta\sigma$ values are extremely low and amount to about 10^{-6}–5×10^{-4} of the magnetization of the sample of $\sigma \approx 4$ A m^2/kg and the characteristic magnetization relaxation times are about 0.1–10 s. The observed experimental features are interpreted within the model of an impurity center, i.e., a complex containing the Fe^{2+} ion. Probably, illumination causes the redistribution of the populations of sublevels of the main Fe^{2+} multiplet such that the strongly anisotropic level is predominantly populated. In this case, the interaction of the impurity subsystem with the matrix crystal changes, leading to the change in the magnetic sublattice canting angle. Different peaks are related to the contributions of the Fe^{2+} ions located in different crystallographic sites relative to the magnetic field direction.

CONCLUSIONS

The SQUID magnetometer developed at the Kirensky Institute of Physics, Siberian Branch, Russian Academy of Sciences, makes it possible to carry out fundamental investigations of both the static mag-

netic properties of various crystalline and film materials and photoinduced changes in the magnetization. In some cases, the author's magnetic measurement technique ensures more accurate and reliable scientific results than those obtained on commercial devices.

FUNDING

This study was supported by the Russian Foundation for Basic Research, the Government of Krasnoyarsk Krai, and the Krasnoyarsk Territorial Foundation for Support of Scientific and R&D Activity, project no. 17-42-240080 "Study of the Effect of the Size, Morphology, and Fabrication Technology on the Functional Properties of Biomagnetic Nanodevices Based on 3*d* Metals and Their Oxides."

CONFLICT OF INTEREST

The author declares no conflict of interest.

REFERENCES

1. Barone, A. and Paternó, G., *Physics and Applications of the Josephson Effect*, Chichester: Wiley, 1982.
2. Clarke, J., Goubau, W.M., and Ketchen, M.B., Tunnel junction dc SQUID: fabrication, operation, and performance, *J. Low Temp. Phys.*, 1976, vol. 25, nos. 1–2, pp. 99–144.
3. Petrakovskii, G.A., Sablina, K.A., Velikanov, D.A., Vorotynov, A.M., Volkov, N.V., and Bovina, A.F., Weak ferromagnetism in copper metaborate CuB_2O_4, *Phys. Solid State*, 1999, vol. 41, no. 7, pp. 1157–1161.
4. Balaev, D.A., Bayukov, O.A., Eremin, E.V., Molokeev, M.S., Pankrats, A.I., Sablina, K.A., Velikanov, D.A., and Vorotynov, A.M., Synthesis and magnetic properties of β-$Cu_3Fe_4(VO_4)_6$ single crystals, *Solid State Phenom.*, 2015, vols. 233–234, pp. 137–140.
5. Patrin, G.S., Beletskii, V.V., Velikanov, D.A., Bayukov, O.A., Vershinin, V.V., Zakieva, O.V., and Isaeva, T.N., Nonstoichiometry and low-temperature magnetic properties of FeSi crystals, *Phys. Solid State*, 2006, vol. 48, no. 4, pp. 700–704.
6. Patrin, G.S., Vas'kovskii, V.O., Velikanov, D.A., and Svalov, A.V., Influence of magnetic field on the interlay er interaction in $(Co/Si/Gd/Si)_n$ films, *JETP Lett.*, 2002, vol. 75, no. 3, pp. 159–161.
7. *Magnetic Property Measurement System. MPMS MultiVu Application User's Manual, Part Number 1014-110C*, San Diego: Quantum Design, 2004.
8. Stepanova, E.A., Volegova, E.A., Kulikova, T.V., Smirnova, E.V., and Volegov, A.S., Investigation of the residual field in the superconducting solenoid of MPMS-XL-7, *Proc. 7th Baikal Int. Conf. "Magnetic Materials. New Technologies" (BICMM–2016), Abstracts of Papers*, Listvyanka, 2016, pp. 220–221.
9. da Luz, M.S., dos Santos, C.A.M., Machado, A.J.S., and Ferreira, B., Diamagnetism and structural transition in the $Ba_2Cu_3O_4Cl_2$ compound, *Braz. J. Phys.*, 2002, vol. 32, no. 3, pp. 744–747.
10. Scheike, T., Böhlmann, W., Esquinazi, P., Barzola-Quiquia, J., Ballestar, A., and Setzer, A., Can doping graphite trigger room temperature superconductivity? Evidence for granular high-temperature superconductivity in water-treated graphite powder, *Adv. Mater.*, 2012, vol. 24, no. 43, pp. 5826–5831.
11. Rabinovich, K.S., Zhuravleva, A.S., Samoilenko, L.L., and Shneider, A.G., Anomalous diamagnetic transitions in $Ba_2Cu_3O_4Cl_2$ and $Sr_2Cu_3O_4Cl_2$ antiferromagnets, *JETP Lett.*, 2013, vol. 98, no. 12, pp. 813–815.
12. Konczykowski, M., Yeshurun, Y., Klein, L., Yacoby, E.R., Chikumoto, N., Vinokur, V.M., and Feigel'man, M.V., Flux pinning by columnar defects in high-temperature superconducting crystals, *J. Alloys Compd.*, 1993, vol. 195, pp. 407–410.
13. Gokhfeld, D.M., Balaev, D.A., Popkov, S.I., Shaykhutdinov, K.A., and Petrov, M.I., Magnetization loop and critical current of porous Bi-based HTS, *Phys. C* (Amsterdam), 2006, vol. 434, no. 2, pp. 135–137.
14. Velikanov, D.A., Rabinovich, K.S., and Samoilenko, L.L., Magnetic properties of $Ba_2Cu_3O_4Cl_2$, *Proc. VI Euro-Asian Symposium "Trends in Magnetism" (EASTMAG-2016), Abstracts of Papers*, Krasnoyarsk: Kirensky Inst. Phys., Sib. Branch, Russ. Acad. Sci., 2016, p. 158.
15. Pejaković, D.A., Kitamura, C., Miller, J.S., and Epstein, A.J., Photoinduced magnetization in the organic-based magnet $Mn(TCNE)_x \cdot y(CH_2Cl_2)$, *Phys. Rev. Lett.*, 2002, vol. 88, no. 5, art. ID 057202.
16. Bahadur, D., Desplanches, C., Rajakumar, S., and Létard, J.-F., Magnetic and photomagnetic studies in nanocrystalline $Ni_{0.5}Zn_{0.5}Fe_{1.7}Co_{0.3}O_4$, *J. Appl. Phys.*, 2008, vol. 103, no. 7, art. ID 07B724.
17. Patrin, G.S., Velikanov, D.A., and Petrakovskii, G.A., Study of photoinduced magnetism in crystals on a SQUID magnetometer, *JETP*, 1993, vol. 76, no. 1, pp. 128–137.

Translated by E. Bondareva